Letter

Possible cluster states in heavy and superheavy nuclei

Jianghua Jia and Yibin Qian[*]

Department of Applied Physics, Nanjing University of Science and Technology, Nanjing 210094, China

Zhongzhou Ren[†]

School of Physics Science and Engineering, Tongji University, Shanghai 200092, China

The α-core structure has been constructed to successfully interpret the band spectra of a series of nuclei above the double shell closure, plus the extension to the heavier cluster structure in the actinide region. By refining the binary cluster model, we show that such kind of picture can be applicable to more heavy nuclei, implying that there can exist cluster states in any heavy nuclei. As for superheavy nuclei, the involved cluster, analogous to the heavy particle radioactivity, is allowed to be above $Z > 28$ plus the core ^{208}Pb. In this sense, besides some predictions on energy spectra of cluster states in superheavy nuclei, the very recently reported 2^+ state of ^{282}Cn is diagnosed to be not in the ground state rotational band via the present method. During the whole procedure, the uncertainty of the cluster model is determined for the first time, by the nonparametric resampling strategy, to make the whole theoretical results reliable and complete.

From the universe to the fundamental particle world, basic objects often behave in an aggregative way, like the assemblage of stars into galaxies or a certain number of quarks confined in hadrons. Accordingly, despite the complicated nature of the nuclear many-body system, the atomic nucleus often exhibits regular patterns, of which clustering is one essential dynamical feature [1]. Actually, the α cluster was, as early as the beginning stage of nuclear physics, taken as the building block to construct $N\alpha$ nuclei or other nuclei with the help of extra particles [2,3]. Since then, clustering has been a key concept to understand the exotic structure in light nuclei [4,5], like the molecularlike band in the beryllium and calcium isotopes [6–8], and especially the famous Hoyle state of ^{12}C [9]. Following the proposal of the Ikeda diagram [10], various cluster configurations were predicted to emerge near the cluster threshold energies for light nuclei. The microscopic cluster models have been then developed to describe significant observables in light nuclei [11], such as the the resonating group method (RGM), generator coordinate method (GCM), or orthogonality condition model (OCM). Moreover, extensive efforts are being devoted to fully and further understanding the cluster structure of light and medium nuclei from both theoretical and experimental aspects [1,12,13].

As for heavier nuclei above ^{100}Sn, one dominant decay channel is α decay [14], which is usually considered as a preformed α cluster subsequently tunneling through the Coulomb barrier. In this sense, the α decay process can be a natural laboratory for probing into the clustering phenomenon of heavy

nuclei [15,16]. However, this is still based on theoretical judgment, while the observation of α-cluster formation in heavy nuclei has been not explicitly implemented. Fortunately, the formation of α clusters has been very recently "seen" at the surface of neutron-rich tin isotopes for the first time via the quasifree α cluster knockout reactions [17]. On the other hand, one could imagine that, besides the α decay process corresponding to the resonant α-core state, there would exist α cluster structure in heavy nuclei demonstrated by their band spectra, esspecially above the double shell closure. Indeed, this was soon realized by Buck *et al.* after a significant α cluster component was proposed for accurately calculating the absolute α decay width of ^{212}Po [18]. Meanwhile, some observed enhanced $E1$ transitions, involving unnatural-parity states of ^{212}Po, have been explained by the "$\alpha + {}^{208}$Pb" clustering case [19]. The α cluster states have been investigated in other nuclei above double-shell closures as well, like ^{20}Ne, ^{44}Ti, ^{94}Mo, and so on [20–23]. Exotic cluster states have also been postulated in actinide nuclei to describe their ground-state rotational bands plus related electromagnetic properties [24,25]. With these in mind, one may say that the cluster is a crucial degree of freedom in curving the dynamical behavior and reaction features of not only light but also heavy nuclei. Consequently, the cluster configuration has been embodied into the shell-model framework [26] and the microscopic cluster model [27], in order to well reproduce the experimental decay width and understand special structural properties.

One main aim of the present study is therefore to shed some light on an open question on the cluster state structure: Are there other kinds of cluster states in heavy nuclei besides ^{212}Po? One decade ago, the concept of cluster decay was changed to allow heavier clusters above $Z = 28$ emitting

*qyibin@njust.edu.cn

†zren@tongji.edu.cn

from superheavy nuclei (SHN) and residual daughters around ^{208}Pb [28,29]. Analogously, one can ask whether there exist heavier cluster states in superheavy nuclei. Meanwhile, an excited 2^+ state in ^{282}Cn was very recently reported, providing us an excellent opportunity to examine the present cluster model in SHN [30]. On the other hand, consensus on the nuclear effective interactions is still far away from being achieved, resulting in the formidable systematic uncertainties. Moreover, there is always the fitting process of model parameters to experiments from the phenomenological point of view, resulting in uncertainties as well as their propagation regarding the model prediction [31]. This issue seems to be missing in the previous studies of the effective cluster model. With these in mind, it is necessary to perform a deep investigation on the cluster states of heavier nuclei beyond the conventional target, plus the evaluation of uncertainties.

The cluster-core relative motion, in the binary cluster model (BCM), is the essential factor to interpret the rotational band spectra of target nuclei. In fact, there is no new story in solving the Schrödinger equation of such a two-body system. The key point is the interaction potential between the cluster and the residual nucleus, which regulates the behavior of the relative motion wave function. As is well known, the nuclear force is not fully recognized at all up to now so that there are various proposals on the cluster-core effective potential. Since the pioneer work on this issue by Buck *et al.* [20], various geometries of cluster-core potential have been proposed in a phenomenological way [22,32], while the semimicroscopic double folding procedure is also employed to construct the two-body potential [33–35]. However, the problem is that an angular-momentum-related factor or radius parameter should be introduced into the nuclear potential for each energy level of studied nuclei, which seems to be not physically reasonable. This is actually caused by the strategy of requiring that the Pauli principle is satisfied by the introduction of the Wildermuth condition, in which the constituent particles of a cluster are supposed to come from the shell-model orbitals above the closed core. To overcome this dilemma, the mixed Woods-Saxon (W.S.) form is then generated to refine the shape of the strong nuclear potential, giving rise to a simultaneous correspondence with half-lives of charged-particle emissions and spectra [24]. Meanwhile, an alternative improvement on the double-folding potential can be reached by including the nuclear medium effect, regulating the behavior of the cluster-core potential at the overlapping region [36]. In this study, we choose a slightly modified version of the mixture of the conventional W.S. potential [23,24] as the nuclear part of the cluster-core potential, namely the (1+Gaussian)(W.S. + W.S.^{3}) shape,

$$V_N = -V_0 \left[1 + \lambda \exp\left(-\frac{r^2}{\sigma^2}\right) \right]$$
$$\times \left\{ \frac{x}{1 + \exp[(r-R)/a]} + \frac{1-x}{1 + \exp[(r-R)/3a]^3} \right\}.$$

$$(1)$$

The coulomb potential V_C is taken to arise from a cluster interacting with a uniformly charged core of radius R. The total

cluster-core potential is then obtained as the sum of these two parts, i.e., $V(r) = V_N(r) + V_C(r)$. The energy spectra can be readily displayed, once the Schrödinger equation, corresponding to the cluster-core relative motion, is solved within this total potential. As mentioned above, the ingredient nucleons of the cluster must lie in the orbitals outside the residual core, which is restricted by the Wildermuth condition,

$$G \geqslant 2n + \ell = \sum_i \left(g_i^{A_d + A_c} - g_i^{A_c} \right). \tag{2}$$

Here the $g_i^{A_d + A_c}$ are the oscillator quantum numbers of the nucleon forming the cluster above the core nucleus, while the $g_i^{A_c}$ are the interior quantum numbers of the A_c nucleons for the cluster in the shell-model context. In this way, the global quantum number G is determined, and the number n of the internal nodes in the radial wave function is subsequently obtained for each angular momentum ℓ. Now let us recall the parameters involved in the nuclear potential (1). As compared to previous studies [22–24], the chosen procedure of these parameters is different here to make the following calculation consistent and steady. Specifically, the subtle radius parameter R is determined by exactly reproducing the yrast bandhead 0^+ of each nucleus, while the residual parameters are completely fixed by matching the ground-state bands of selected nuclei, namely ^{20}Ne, ^{44,52}Ti, ^{60}Zn, ^{94}Mo, ^{136}Te, and ^{212}Po.

One objective of this study, as mentioned before, is the evaluation of uncertainty of the present BCM. In fact, the issue on the uncertainty has recently received special attention in the field of nuclear physics through statistical methods like sensitivity analysis and Bayesian inference [31,37–40]. Besides, the Monte Carlo bootstrap tool [41], as a nonparametric resampling method, has been widely accepted in the statistics practice and machine learning strategies due to its robustness and efficiency [42–45]. The applicability of this method has been also shown in simulating NN scattering data [46] and the estimation of α decay half-lives [47]. In the present study, the number of samples in the statistical analysis is relatively limited, corresponding to the above listed nuclei as the learning set. Moreover, the bootstrap method can provide standard error and bias estimates of the involved model parameters and given measured observables without prior assumptions such as normal distributions. Considering these, it is suitable and necessary to bootstrap the α-cluster state bands of typical nuclei, aiming at a global description and prediction on possible cluster states of heavy and superheavy nuclei. The specific steps are listed as follows:

(i) The ground-state (g.s.) bands, from 2^+ to 10^+, of the aforementioned α-core-type nuclei are selected as the learning data set, namely $\{E_k\}$ with the total number of N. Given the high accuracy of these measured data, they are considered as accurate values. By resampling and allowing replacement (an important choice in the bootstrap method), one can always pick up N samples from the learning set $\{E_k\}$. One can then obtain an energy array $\{E_{k'}^i\}$ for the ith resampling, and this process will be repeated again and again to get $M = 10^5$ groups of $\{E_{k'}^i\}$ with the computational facility.

TABLE I. The correlation coefficients of the parameter set involved in the effective nuclear potential.

	V_0	a	x	λ	σ
V_0	1.000				
a	-0.8257	1.000			
x	-0.6699	0.9272	1.000		
λ	-0.0271	0.0888	0.0797	1.000	
σ	-0.7015	0.4572	0.4307	-0.4221	1.000

(ii) For each group of $\{E_{k'}^i\}$, the parameter set involved in the cluster-core potential will be determined through the differential evolution algorithm [48], by minimizing the square deviation between the experimental energy levels and the calculated results, namely

$$\chi_i^2 = \frac{\sum_{i=1}^N \left(E_{k',\text{cal}}^i - E_{k',\text{exp}}^i\right)^2}{N}. \quad (3)$$

In this way, there will be M groups of parameter sets, plus the corresponding $E_{k,\text{cal}}^i$ derived from the ith optimal parameter set, to be stored for the following analysis.

(iii) With the help of the above parameter groups, the uncertainty evaluation on the nuclear potential and the sequential prediction can proceed via the statistical bootstrap strategy. The target observable in this study is the energy level, whose uncertainty is deduced from the systematical and statistical aspects. The systematical uncertainty of one energy level, rooted in the model itself, is determined by

$$\hat{\sigma}_{sys,k}^2 = \left(\bar{E}_{k,\text{cal}} - E_{k,\text{exp}}^i\right)^2, \quad (4)$$

where $\bar{E}_{k,\text{cal}}$ is the mean value of the calculated results for the kth energy level in the learning set, i.e., $\bar{E}_{k,\text{cal}} = \frac{1}{M}\sum_{i=1}^M E_{k,\text{cal}}^i$. On the other hand, the statistical error is assessed by the unbiased square deviation of the calculated energy levels themselves, namely

$$\hat{\sigma}_{stat,k}^2 = \frac{1}{M-1}\sum_{i=1}^M \left(E_{k,\text{cal}}^i - \bar{E}_{k,\text{cal}}\right)^2. \quad (5)$$

The model uncertainty of the kth energy level is then obtained as $\hat{\sigma}_{total,k}^2 = \hat{\sigma}_{sys,k}^2 + \hat{\sigma}_{stat,k}^2$, leading to the total uncertainty of the whole learning set, namely

$$\hat{\sigma}_{total}^2 = \frac{1}{N}\sum_{k=1}^N \hat{\sigma}_{total,k}^2 = \frac{1}{N}\sum_{k=1}^N \left(\hat{\sigma}_{sys,k}^2 + \hat{\sigma}_{stat,k}^2\right). \quad (6)$$

Based on the obtained M groups of parameters, one can easily obtain correlation coefficients between parameters, which are shown in matrix form in Table I. As expected, the Gaussian term of Eq. (1) regulates the spacing between the 0^+ and 2^+ states, while it is not relevant to the higher-lying states [22]. The strength parameter λ is indeed in tiny connection with other parameters, and the σ is more sensitive to the depth V_0 for a better pattern in the beginning region.
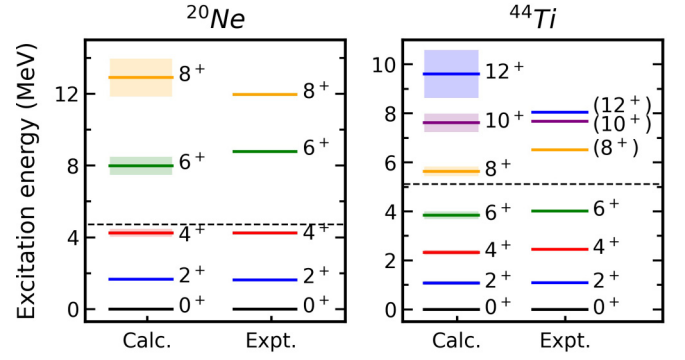

FIG. 1. The g.s. bands of ^{20}Ne and ^{44}Ti, in which the uncertainty bar is denoted by the shadow range. The dash line indicates the α+core breakup threshold.

The three parameters of the W.S. part are correlated with each other to determine the suitable geometry of the final nuclear potential. As is well known, the electromagnetic transition probability, apart from the spectra, is another quantity that is very sensitive to the structure of nuclear states. Once the cluster-core potential is determined within one sampled group of parameters, the radial wave functions are obtained. In the BCM scheme plus the present case of spinless clusters and cores, the reduced transition strength $B(E2 \downarrow)$ can be then given by [24,25]

$$B(E2; J \to J-2) = \frac{15\beta^2}{8\pi}\frac{J(J+1)}{(2J+1)(2J-1)}\langle r_{J,J-2}^2\rangle^2 \quad (7)$$

with

$$\beta = \frac{Z_c A_d^2 + Z_d A_c^2}{(A_d + A_c)^2}, \quad (8)$$

$$\langle r_{J,J-2}^2\rangle = \int_0^\infty u_J^*(r)r^2 u_{J-2}(r)dr. \quad (9)$$

Here the subscripts c and d separately correspond to the cluster and the residual core, and the radial wave function $u_J(r)$ comes from the cluster state with the angular momentum J. Note that there is no introduction of any effective charge.

For an intuitive judgment of the present BCM, the comparison of the experimental energy levels with the computed values are initially plotted in Fig. 1 for two light nuclei ^{20}Ne and ^{44}Ti, while those of two heavier nuclei ^{94}Mo and ^{212}Po are shown in Fig. 2. The evaluated uncertainty, corresponding to one standard deviation $\hat{\sigma}$ around the most probable value, is also demonstrated by the shadow for each level. As one can see from these two figures, the g.s. spectra are quite well reproduced for both the light and heavy nuclei, while the uncertainty appears to increase with increasing angular momentum and mass number. For example, the largest total uncertainty occurs in the 12^+ state of ^{44}Ti. This may come from the nonlocality of the valence nucleons in the high-lying state for light nuclei [12,49], which seems to be not satisfied by the BCM framework. On the other hand, there are overlaps between the uncertainty bars of two neighboring energy levels for the high-lying states, plus the more serious tendency towards heavy nuclei. In this sense, quantum "chaos" would
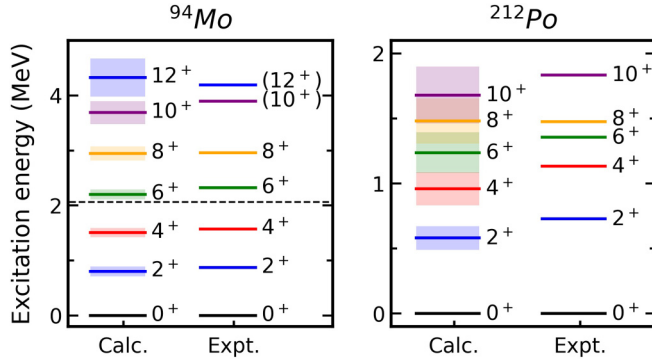
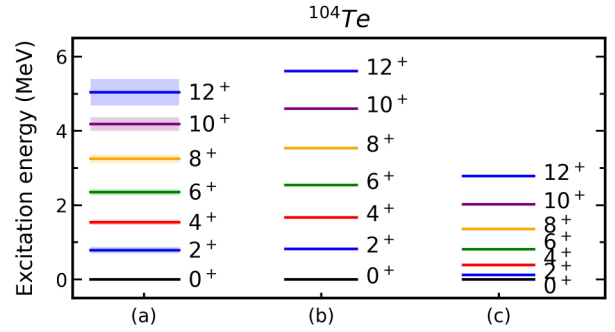FIG. 2. Same as Fig. 1 but for heavier nuclei ^{94}Mo and ^{212}Po.

FIG. 3. Calculated energy levels for the ground state band of ^{104}Te in terms of the $\alpha + {}^{100}$Sn system, in comparison with the other theoretical spectra in panel (b) from Ref. [23] and in panel (c) from Ref. [35].

exist in the BCM prediction for the high-lying rotational states of heavy nuclei. Hence the evaluation of these energy regions is not shown here except for ^{212}Po. The obvious uncertainty and overlap of this typical nucleus raises questions on the capability of the BCM for the heavy and superheavy nuclei, which will be tackled in the following. Despite this, the total uncertainty is actually only 0.196 MeV for the whole learning set. On further examination, the calculated $B(E2)$ values are compared with the available experimental data for the above target nuclei in Table II. Within the aforementioned bootstrap treatment, the statistical uncertainty is also presented for the reduced transition strength. Obviously, the measured $B(E2)$ value and the general trend are satisfactorily reproduced by the BCM despite the overestimation in ^{212}Po. This latter abnormal case may be understood from the natural thought that the mean-field effect will be enhanced for heavy nuclei as compared to lighter ones. In this sense, the strong spin-orbit force can at least moderate the α cluster correlation when proceeding to heavier nuclei, resulting in the relatively large $B(E2)$ value without the consideration of single-nucleon degree. We then apply the BCM, plus the uncertainty eval-

TABLE II. Comparison of the experimental data and the calculated values for the reduced $E2$ transition strength of four nuclei, namely ^{20}Ne, ^{44}Ti, ^{94}Mo, ^{212}Po. Note that only the transitions with experimental data are listed here.

Nuclei	Transition	$B(E2\downarrow)_{\text{expt}}$ $(e^2\text{fm}^4)$	$B(E2\downarrow)_{\text{calc}}$ $(e^2\text{fm}^4)$
^{20}Ne	$2^+ \rightarrow 0^+$	66 ± 3	49.3 ± 14.5
	$4^+ \rightarrow 2^+$	71 ± 6	66.4 ± 22.5
	$6^+ \rightarrow 4^+$	65 ± 10	57.3 ± 23.6
	$8^+ \rightarrow 6^+$	29 ± 4	33.9 ± 19.5
^{44}Ti	$2^+ \rightarrow 0^+$	120 ± 37	103.8 ± 29.4
	$4^+ \rightarrow 2^+$	277 ± 46	140.9 ± 42.6
	$6^+ \rightarrow 4^+$	157 ± 22	133.1 ± 42.8
	$8^+ \rightarrow 6^+$	>14	106.6 ± 37.1
	$10^+ \rightarrow 8^+$	138 ± 28	71.1 ± 27.4
	$12^+ \rightarrow 10^+$	<60	33.9 ± 14.6
^{94}Mo	$2^+ \rightarrow 0^+$	406 ± 10	201.3 ± 58.4
	$4^+ \rightarrow 2^+$	660 ± 101	278.4 ± 84.0
^{212}Po	$6^+ \rightarrow 4^+$	293 ± 83	729.9 ± 251.4
	$8^+ \rightarrow 6^+$	173 ± 7	694.3 ± 236.7
	$10^+ \rightarrow 12^+$	165 ± 45	626.7 ± 210.4

uation, to the superallowed α emitter ^{104}Te [50]. Due to the lack of experimental data, the calculated energy levels are compared with other theoretical results [23,35] in Fig. 3. The predicted energies in the panel (b) are produced by the BCM with a different fitting procedure [23]. In detail, the low-lying energy band, in Ref. [23], is generally consistent with that of the present results, while there is an obvious deviation with respect to higher-lying states. In panel (c), the nuclear potential is derived from the double-folding integral [35], leading to a narrow rotational band. Given the extensive efforts devoted to experiments around the tin region [17,50], it is expected that the present prediction can be examined in the near future.

As mentioned before, another objective in this study is to explore the possible cluster states in heavy and superheavy nuclei with $N > 126$. Within the BCM, the residual core, analogous to the choice in the regular cluster emission of actinide nuclei [24] and the heavy particle decay of superheavy nuclei [28], is considered to be the double-magic nucleus ^{208}Pb. The other component is then extended from α particle to carbon, oxygen, neon, and heavier clusters. Before this procedure, we paid special attention to the choice of the fundamental nuclear potential, especially considering the aforementioned situation in ^{212}Po. This is due to the fact the number n of the internal nodes in the wave function would be quite large ($\approx$200), and this kind of oscillation should be performed in an extremely narrow range. Meanwhile, the wave function behavior is exactly responsible for the reasonable description of the energy spectra. In fact, the interior region of the cluster-core potential generally behaves like a relatively stable plateau, which results in a sine or cosine type of radial wave function. One can then easily get the point that the angular frequency, corresponding to the node number, is related to the wave number $\sqrt{2\mu(V-E)/\hbar^2}$. Given that the total potential $V(r)$ varies quite limitedly when $r < R$, this steady value of $(V - E)$ is proportional to the depth parameter V_0, leading to the relationship $\sqrt{\mu V_0} \propto n$. Considering that the reduced mass number μ can be approximated by the cluster mass number A_c, the depth of the nuclear potential can be regulated by

$$\frac{V_0}{A_c} = V_1 \frac{n^2}{A_c^2} + V_2 \frac{n}{A_c} + V_3. \quad (10)$$
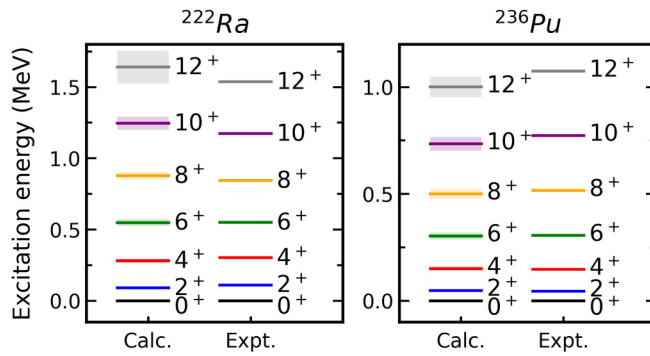
FIG. 4. Similar to Figs. 1 and 2, but with the refined IBCM for the heavier cluster states above ^{208}Pb. Note that the rotational band has been located in a quite narrow energy range.

With such an improved BCM (IBCM), we explore the rotational spectra in the actinide region, to be the benchmark for the attempt to probe into the cluster structure of superheavy nuclei. Initially, the experimental rotational spectra are also well reproduced for the Ra, U, and Th isotopes in terms of the C, O, and Ne cluster structures above ^{208}Pb. The standard deviation is around 0.06 MeV for this fitting procedure, positively confirming the validity of the present construction. In addition, we have also expanded the target to the heavier Mg and Si cluster cases as a test, accompanied by high accuracy. As typical examples, the energy levels of ^{220}Ra and ^{236}Pu are presented in Fig. 4, where the calculated energies not only agree quite well with the measured values, but also carry very narrow uncertainty ranges. Encouraged by this, the IBCM is applied to predict the possible cluster structure of superheavy nuclei, while the 2_1^+ state has been recently postulated in ^{282}Cn. As a result, we pay special attention to g.s. rotational bands of ^{282}Cn. The 2^+ state is found to lie around 0.02 MeV, deviating from the reported value (about 0.22 MeV) for the 2_1^+ state. One may therefore conclude that this reported excited state cannot be divided into the pure g.s. rotational band or the present choice of the two-body cluster structure should be reconsidered. It is hoped that this study can be further checked in future spectra experiments of superheavy nuclei.

In conclusion, we have performed the uncertainty analysis on the g.s. rotational bands of all the α-core-type nuclei within the binary cluster model for the first time, to validate the applicability of the BCM for exploring the possible cluster states in heavy and superheavy nuclei. These involved transition strengthes $B(E2)$ can be well reproduced along with statistical uncertainties as well. Through proposing a subtle constraint on the depth of the nuclear potential and the nodes of the cluster-core radial wave function, we have further refined the BCM to adjust the g.s. rotational spectra of heavy nuclei around the core ^{208}Pb. These experimental energy levels are not only reproduced very well but also with quite narrow uncertainties, demonstrating the reliability of the present development of the cluster model. On the other hand, the presently reported cluster states can serve as the basis to understand the cluster formation amplitude and the absolute decay width. The recently observed 2_1^+ state in ^{282}Cn is also discussed in terms of the present IBCM, and it is hoped that the present study can enlarge our knowledge of the cluster state band all over the nuclear chart.

[1] M. Freer, H. Horiuchi, Y. Kanada-En'yo, D. Lee, and Ulf-G. Meißner, Rev. Mod. Phys. **90**, 035004 (2018).

[2] G. Gamow, Proc. R. Soc. London A **126**, 632 (1930).

[3] J. A. Wheeler, Phys. Rev. **52**, 1107 (1937).

[4] M. Freer, Rep. Prog. Phys. **70**, 2149 (2007).

[5] W. von Oertzen, M. Freer, and Y. Kanada-En'yo, Phys. Rep. **432**, 43 (2006).

[6] Z. H. Yang, Y. L. Ye, Z. H. Li, J. L. Lou, J. S. Wang, D. X. Jiang, Y. C. Ge, Q. T. Li, H. Hua, X. Q. Li, F. R. Xu, J. C. Pei, R. Qiao, H. B. You, H. Wang, Z. Y. Tian, K. A. Li, Y. L. Sun, H. N. Liu, J. Chen *et al.*, Phys. Rev. Lett. **112**, 162501 (2014).

[7] W. Jiang, Y. L. Ye, C. J. Lin, Z. H. Li, J. L. Lou, X. F. Yang, Q. T. Li, Y. C. Ge, H. Hua, D. X. Jiang, D. Y. Pang, J. Li, J. Chen, Z. H. Yang, X. H. Sun, Z. Y. Tian, J. Feng, B. Yang, H. L. Zang, Q. Liu *et al.*, Phys. Rev. C **101**, 031304(R) (2020).

[8] Y. Liu, Y. L. Ye, J. L. Lou, X. F. Yang, T. Baba, M. Kimura, B. Yang, Z. H. Li, Q. T. Li, J. Y. Xu, Y. C. Ge, H. Hua, J. S. Wang, Y. Y. Yang, P. Ma, Z. Bai, Q. Hu, W. Liu, K. Ma, L. C. Tao *et al.*, Phys. Rev. Lett. **124**, 192501 (2020).

[9] M. Freer and H. O. U. Fynbo, Prog. Part. Nucl. Phys. **78**, 1 (2014).

[10] K. Ikeda, N. Takigawa, and H. Horiuchi, Prog. Theor. Phys. Suppl. E**68**, 464 (1968).

[11] H. Horiuchi, Prog. Theor. Phys. Suppl. **62**, 90 (1977).

[12] Z. Ren and B. Zhou, Front. Phys. **13**, 132110 (2018).

[13] A. Tohsaki, H. Horiuchi, P. Schuck, and G. Röpke, Rev. Mod. Phys. **89**, 011002 (2017).

[14] C. Qi, R. Liotta, and R. Wyss, Progr. Part. Nucl. Phys. **105**, 214 (2019).

[15] D. S. Delion, A. Sandulescu, and W. Greiner, Phys. Rev. C **69**, 044318 (2004).

[16] D. S. Delion and A. Dumitrescu, Phys. Rev. C **102**, 014327 (2020).

[17] J. Tanaka, Z. Yang, S. Typel, S. Adachi, S. Bai, P. van Beek, D. Beaumel, Y. Fujikawa, J. Han, S. Heil, S. Huang, A. Inoue, Y. Jiang, M. Knösel, N. Kobayashi, Y. Kubota, W. Liu, J. Lou, Y. Maeda, Y. Matsuda *et al.*, Science **371**, 260 (2021).

[18] B. Buck, A. C. Merchant, and S. M. Perez, Phys. Rev. Lett. **72**, 1326 (1994).

[19] A. Astier, P. Petkov, M.-G. Porquet, D. S. Delion, and P. Schuck, Phys. Rev. Lett. **104**, 042701 (2010).

[20] B. Buck, C. B. Dover, and J. P. Vary, Phys. Rev. C **11**, 1803 (1975).

[21] S. Ohkubo, Phys. Rev. Lett. **74**, 2176 (1995).

[22] M. A. Souza and H. Miyake, Phys. Rev. C **91**, 034320 (2015).

[23] M. A. Souza, H. Miyake, T. Borello-Lewin, C. A. da Rocha, and C. Frajuca, Phys. Lett. B **793**, 8 (2019).

[24] B. Buck, A. C. Merchant, and S. M. Perez, Phys. Rev. Lett. **76**, 380 (1996).

[25] T. T. Ibrahim, S. M. Perez, S. M. Wyngaardt, B. Buck, and A. C. Merchant, Phys. Rev. C **85**, 044313 (2012).

[26] D. S. Delion and R. J. Liotta, Phys. Rev. C **87**, 041302(R) (2013).

[27] S. Yang, C. Xu, G. Röpke, P. Schuck, Z. Ren, Y. Funaki, H. Horiuchi, A. Tohsaki, T. Yamada, and B. Zhou, Phys. Rev. C **101**, 024316 (2020).

[28] D. N. Poenaru, R. A. Gherghescu, and W. Greiner, Phys. Rev. Lett. **107**, 062503 (2011).

[29] D. N. Poenaru, R. A. Gherghescu, and W. Greiner, Phys. Rev. C **85**, 034615 (2012).

[30] A. Såmark-Roth, D. M. Cox, D. Rudolph, L. G. Sarmiento, B. G. Carlsson, J. L. Egido, P. Golubev, J. Heery, A. Yakushev, S. Åberg, H. M. Albers, M. Albertsson, M. Block, H. Brand, T. Calverley, R. Cantemir, R. M. Clark, C. E. Düllmann, J. Eberth, C. Fahlander *et al.*, Phys. Rev. Lett. **126**, 032503 (2021).

[31] J. D. McDonnell, N. Schunck, D. Higdon, J. Sarich, S. M. Wild, and W. Nazarewicz, Phys. Rev. Lett. **114**, 122501 (2015).

[32] B. Buck, A. C. Merchant, and S. M. Perez, Phys. Rev. Lett. **65**, 2975 (1990).

[33] F. Hoyler, P. Mohr, and G. Staudt, Phys. Rev. C **50**, 2631 (1994).

[34] P. Mohr, Eur. Phys. J. A **53**, 209 (2017).

[35] D. Bai and Z. Ren, Eur. Phys. J. A **54**, 220 (2018).

[36] D. Deng and Z. Ren, Phys. Rev. C **96**, 064306 (2017).

[37] J. Toivanen, J. Dobaczewski, M. Kortelainen, and K. Mizuyama, Phys. Rev. C **78**, 034306 (2008).

[38] J. Dobaczewski, W. Nazarewicz, and P. Reinhard, J. Phys. G: Nucl. Part. Phys. **41**, 074001 (2014).

[39] N. Schunck, J. D. McDonnell, D. Higdon, J. Sarich, and S. M. Wild, Eur. Phys. J. A **51**, 169 (2015).

[40] R. Furnstahl, D. Phillips, and S. Wesolowski, J. Phys. G: Nucl. Part. Phys. **42**, 034028 (2015).

[41] B. Efron, *The Jackknife, the Bootstrap and Other Resampling Plans* (SIAM, Philadelphia, 1982).

[42] B. LeBaron and A. S. Weigend, IEEE Trans. Neural Networks **9**, 213 (1998).

[43] J. Kybic, IEEE Trans. Image Process. **19**, 64 (2009).

[44] E. Zio, IEEE Trans. Nucl. Sci. **53**, 1460 (2006).

[45] R. Wehrens, H. Putter, and L. M. Buydens, Chemomr. Intell. Lab. Syst. **54**, 35 (2000).

[46] R. N. Pérez, J. Amaro, and E. R. Arriola, Phys. Lett. B **738**, 155 (2014).

[47] B. Cai, G. Chen, J. Xu, C. Yuan, C. Qi, and Y. Yao, Phys. Rev. C **101**, 054304 (2020).

[48] R. Storn and K. Price, in *Proceedings of IEEE International Conference on Evolutionary Computation*, Nagoya, 1996 (IEEE, Piscataway, NJ, 1996), pp. 842–844.

[49] B. Zhou, Y. Funaki, H. Horiuchi, Z. Ren, G. Röpke, P. Schuck, A. Tohsaki, C. Xu, and T. Yamada, Phys. Rev. Lett. **110**, 262501 (2013).

[50] K. Auranen, D. Seweryniak, M. Albers, A. D. Ayangeakaa, S. Bottoni, M. P. Carpenter, C. J. Chiara, P. Copp, H. M. David, D. T. Doherty, J. Harker, C. R. Hoffman, R. V. F. Janssens, T. L. Khoo, S. A. Kuvin, T. Lauritsen, G. Lotay, A. M. Rogers, J. Sethi, C. Scholey *et al.*, Phys. Rev. Lett. **121**, 182501 (2018).